

# Topological Heterostructures for Spectrally Nearly Constant Intensity Enhancements of Audio Sound and Ultrasonics

Cui-xin Zhang<sup>1,2</sup>, An Chen<sup>1,2</sup>, Wei Hu,<sup>1,2</sup> Jing Yang<sup>1,2,\*</sup>, Bin Liang,<sup>1,2,†</sup> Johan Christensen,<sup>3,‡</sup> and Jian-chun Cheng<sup>1,2</sup>

<sup>1</sup>Key Laboratory of Modern Acoustics, MOE, Institute of Acoustic, Department of Physics, Nanjing University, Nanjing 210093, People's Republic of China

<sup>2</sup>Collaborative Innovation Center of Advanced Microstructures, Nanjing University, Nanjing 210093, People's Republic of China

<sup>3</sup>Department of Physics, Universidad Carlos III de Madrid Leganés, Madrid ES-28916, Spain



(Received 20 April 2023; revised 4 July 2023; accepted 18 July 2023; published 16 August 2023)

Topological interface states and the associated enhancement of sound intensity in periodic systems is of fundamental interest in wave physics and may have wide applications, such as in sound detection and biomedical imaging. Yet their occurrence is hitherto limited to the topological transition where the bands inverse. Here we theoretically design and experimentally demonstrate an “acoustic heterostructure” capable of giving rise to interface states at arbitrary frequency within the topological band gap, which is accomplished by adjusting a single structural parameter. The remarkable sound-intensity enhancement, which reaches  $10^4$ , is not affected by this change but remains near constant within the said frequency range and is tested in both a sonic and an elastic wave setting. We envision our strategy to be useful in the design of alternative acoustic sensors and detectors with high flexibility and sensitivity in diverse scenarios, such as nondestructive detection and medical imaging.

DOI: 10.1103/PhysRevApplied.20.024040

## I. INTRODUCTION

Topological interface mode, which is often considered as the most applicable wave property of the topological insulator, has been extensively studied in electronic, photonic, and acoustic systems in recent years [1–15]. Particularly, phononic crystals, by virtue of the macroscopic nature, have become a vital wave-control playground with flexible designability to demonstrate advanced interface state manipulations [16–21]. Some typical applications are robust one-way transport based on the pseudospin-momentum locking, the acoustic version of type-II Weyl nodes made of one-dimensional (1D) dimerized acoustic resonators and the manipulation of topological interface states in the low-frequency band gap [22–24]. On one-dimensional acoustic systems, many researchers have lately paid their attention to applications of the Su-Schrieffer-Heeger (SSH) model, which can support topological interface states and the associated enhancement of sound intensity [25,26].

Recently, an acoustic heterostructure has been proposed to achieve valley Hall insulators where the high-capacity

transmission is realized by constructing wide-aperture helical waveguide modes [27–31]. However, the wide-aperture topological waveguides still possess a limited application value due to the fixed working frequency range and the decreased working bandwidth as the waveguides widen. The realization of sound-intensity enhancement at multiple frequencies and the modulation of topological interface states based on 1D acoustic heterostructure systems may have wide application prospects.

In this work, we consider an acoustic heterostructure capable of generating topological interface states at arbitrary frequency within the topological band gap. The proposed heterostructure consists of two topological sonic crystals (SCs) with a different band structure. The coupling strength between resonant cavities can be easily adjusted by changing a single structural parameter in the unit cell, which allows the frequency of the interface state to be freely and easily controlled within a broadband. This broadband modulation of the topological interface states enables multifrequency acoustic field enhancement within the topological band gap where the state-intensity enhancement is not affected by its frequency shift. We exemplify the generality of our proposed mechanism by also designing a phononic crystal (PnC) composed of aluminum beams, where also here, a pronounced yet constant local intensity enhancement at shifted frequencies is explored

\* yangj@nju.edu.cn

† liangbin@nju.edu.cn

‡ johan.christensen@uc3m.es

in the ultrasonic regime, which is interesting for sensing, filtering, and imaging purposes.

## II. ACOUSTIC HETEROSTRUCTURE MODEL AND THE TOPOLOGICAL PROPERTY ANALYSIS

The schematic of the proposed acoustic heterostructure is illustrated in Fig. 1(a), which is a 1D system composed of two SCs with different band structures. The unit cell of the SCs is a rectangular waveguide comprising five tubes with expanded or shrunk cross section, filled with air. The lattice constant of the mirror-symmetric unit cell is  $a = 2a_1 + 2a_2 + a_3$ , and the wall of waveguide is acoustically rigid. The geometric and material parameters are listed in Table I. We describe such a one-dimensional system containing two SCs with different band structure as an “acoustic heterostructure” [29]. As shown in Fig. 1(b), the inconsistent band gap width is of vital significance for the effectiveness of the heterostructure we defined. As will be proved later, in our design the parameter of  $a_3$  is physically responsible for the strength of coupling between the resonant cavities on both sides of the interface, offering the easiest possible way to control the frequency of topological interface states. Here we investigate four different SC configurations, denoted as S1, S2, S3, and S4, respectively, with each having the same unit-cell length  $a = 21$  cm but a different  $a_3$ . Specifically, we set  $a_3 = 4.0$  cm for S1, 7.0 cm for S2, 10.0 cm for S3, and 12.0 cm for S4, respectively (as listed in Table II). Throughout the paper, numerical simulations are performed using the commercial software COMSOL Multiphysics.

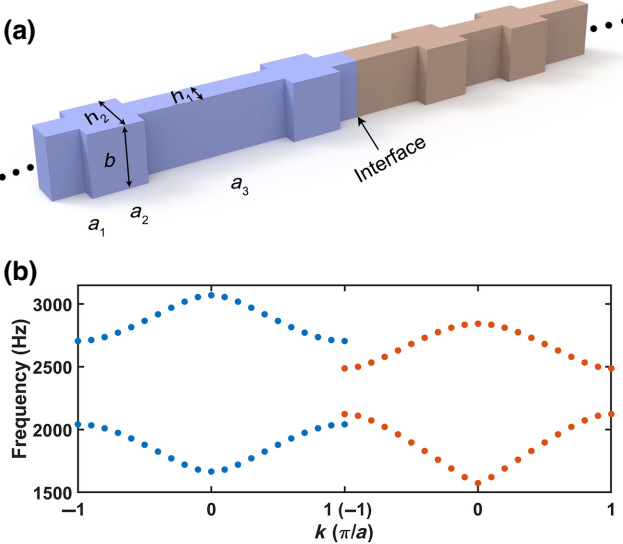


FIG. 1. (a) Schematic diagram of the proposed acoustic heterostructure, which is composed of two SCs with inconsistent band structure shown in (b) marked by dots with respective color.

TABLE I. Geometric and material parameters of the model.

$a$ (cm)	$b$ (cm)	$h_1$ (cm)	$h_2$ (cm)	$\rho$ (kg/m <sup>3</sup> )	$c$ (m/s)
21	4	2	4	1.21	343

The topological properties of a 1D crystal can be characterized by the Zak phase [24,25], and the calculation method for the  $n$ th Bloch band in the dispersion is expressed as follows:

$$\theta_n^{\text{Zak}} = \int_{-\pi/a}^{\pi/a} \left[ i \int_{\text{unit cell}} \frac{1}{2\rho c^2} dx u_{n,k}^*(x) \partial_k u_{n,k}(x) \right] dk, \quad (1)$$

where  $\theta_n^{\text{Zak}}$  is the Zak phase of the  $n$ th band and  $u_{n,k}(x)$  is the cell-period Bloch eigenfunction of a state with a given wave number  $k$ . For the  $n$ th band of a 1D PnC, the wave field is given by  $p(x) = u(x)\exp(ikx)$ . The factor  $1/(2\rho v^2)$  is the weight function of an acoustic system with  $\rho$  and  $v$  being the mass density and the sound speed of air, respectively. On the other hand, the Zak phase of an isolated band in such a 1D system can also be obtained from the symmetry properties of band-edge states. As the unit cell has mirror symmetry with respect to its central cross-section plane, the Zak phase can have only two values: 0 or  $\pi$ . If two states at the center and edge of the Brillouin zone belonging to the same band have the same symmetry—that is, both even or odd with respect to the central plane—then the Zak phase of this band is 0. Otherwise, the Zak phase is  $\pi$  [2,32]. Figure 2(a) shows that their dispersions are exactly the same while their topological phases are different. Compared to the first band gap, the corresponding wavelength in the third band gap is much shorter, which is expected to produce a higher sensitivity with respect to the change of the structural parameters. For a better illustration of our proposed mechanism, therefore, we choose the third band gap as an example where the topological phase changes with the transition from S1 to S3.

We calculate the eigenstates of the unit cell at  $ka/\pi = 1$  of the two associated bands for the third band gap as a function of  $a_3$  and plot typical examples in Fig. 2(b). The red and blue lines indicate the symmetric and antisymmetric eigenstates, respectively. When the value of  $a_3$  changes to the situation of S2 as  $a_3 = 7$  cm, the band gap closes, and the two eigenstates merge to form a topological transition point [33–36]. Notice that the red (blue) states originally

TABLE II. Different geometric configurations of the SCs.

SC	$a_1$ (cm)	$a_2$ (cm)	$a_3$ (cm)
S1	5.0	3.5	4.0
S2	3.5	3.5	7.0
S3	2.0	3.5	10.0
S4	1.0	3.5	12.0

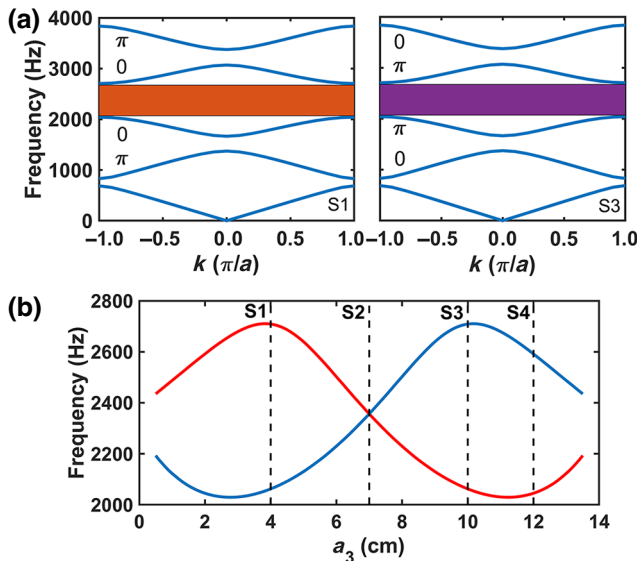


FIG. 2. (a) Band structures of the two geometric configurations S1 and S3, respectively. The orange and purple zones represent the band gaps with different topological properties, but the same band structure. (b) Boundary frequencies ( $ka/\pi$ ) of the third band gap at the edge of the Brillouin zone with variation of  $a_3$ , and a topological transition point occurs at S2.

located above (below) the band gap when  $a_3 < 7$  cm flip to below (above) the band gap when  $a_3 > 7$  cm. A topological band gap is insensitive to certain local perturbations, which shows excellent potential for robust sound isolation.

### III. BROADBAND MODULATION AND ASSOCIATED SOUND INTENSITY ENHANCEMENT IN THE TOPOLOGICAL ACOUSTIC HETEROSTRUCTURE

It is conventionally perceived that as long as the two SCs have distinct topological properties in the common frequency region, the topological interface states will definitely exist [37]. Each unit cell has mirror symmetry with respect to its center plane and the band structure of SCs on both sides of the interface exactly remains identical, characterized as double symmetry. Here, we break the double symmetry showing that the frequencies of the topological interface states are modulated within the topological band gap, where the symmetry in the band structure of two SCs on the left and right sides is no longer held. Since the band gaps of these two SCs have different width, it is reasonable to dub the proposed 1D structure an “acoustic heterostructure.” When we continuously adjust  $a_3$  in the unit cell for the right SC while keeping that for the left SC fixed, the frequencies of the topological interface states is not limited to the touching point and exhibit an obvious shift. Multifrequency topological acoustic field enhancements in the range of the third band gap are achieved due to the breaking of the double symmetry as shown in Fig. 3,

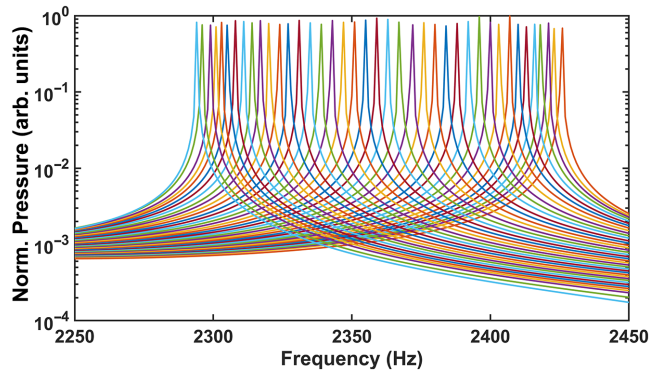
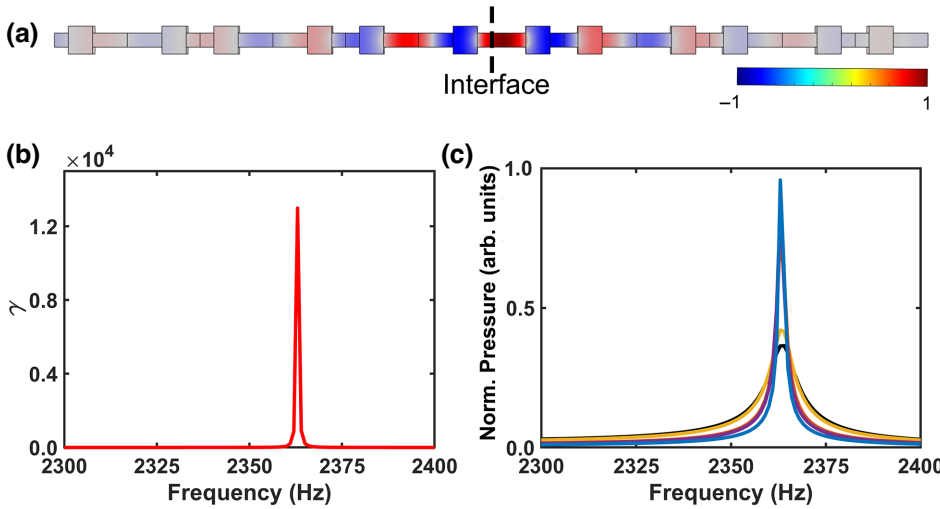


FIG. 3. Multifrequency topological acoustic field enhancement in the special acoustic heterostructure without double symmetry. Broadband modulation of the topological interface state is obtained inside the third band gap.

deviating from the touching point. Of note, the remarkable sound-intensity enhancement is not affected by such a frequency shift (these curves are normalized with one given maximum value), owing to the robustness of preserved topological properties.

In our acoustic heterostructure system, the breaking of the double symmetry introduces different coupling strengths between the resonant cavities of SCs on both sides of the interface, which is dependent on the structural parameter [38,39]. As an acoustical counterpart of the electrical heterostructure, our proposed acoustic heterostructure produces an offset in the frequency of upper and lower edges of the band gap. The topological interface state frequency is shifted within the band-gap range, and thus offers the possibility of modulating acoustic enhancement in a broadband.

A topological phase transition takes place in our 1D acoustic heterostructure system, and Fig. 4(a) shows the simulated topological localized distributions of pressure-field amplitude at the interface in the third band gap. Knowledge of the bulk-band geometric phase in a SC allows us to create topological interface states with a significant acoustic field enhancement state at their interface [40]. Owing to the highly confined spatial characteristics in this 1D system, the sound-intensity enhancement can be observed. In order to quantitatively estimate the enhancement ratio, we introduce a parameter defined as  $\gamma = |P_{\text{topo}}|^2 / |P_{\text{in}}|^2$  where  $|P_{\text{topo}}|^2$  and  $|P_{\text{in}}|^2$  refer to the sound intensity of topological interface state and the input wave in simulation, respectively. The topological interface state appears around the frequency of the touching point at 2360 Hz, and the enhancement ratio exceeds  $10^4$ . Besides, we get different degrees of interface acoustic field enhancement when the two phononic crystals with opposed topological phases maintain the double symmetry, that is, the equivalent band-gap width. Diverse magnitudes of normalized sound-intensity enhancement were obtained



at one topological interface state frequency by varying system parameter  $a_3$  under the double symmetry, as shown in Fig. 4(c).

#### IV. EXPERIMENTAL RESULTS

We further carry out experiments to verify our theoretical predictions and numerical simulations. A photograph of the experimental setup is illustrated in Fig. 5(a). In the measurement, we connect three S1, S4 without the double symmetry as an acoustic heterostructure system and

FIG. 4. (a) Simulated amplitude of pressure-field distributions for interface state in the third band gap. (b) The enhancement ratio  $\gamma$  at the interface state. An amplification by a factor of over  $10^4$  is observed. (c) Under the double symmetry, different degrees of sound-intensity enhancement can be observed at one topological interface state with the change of  $a_3$ .

S1, S3 protected by the double symmetry, respectively. All SC samples were fabricated using three-dimensional (3D) printing. Polylactic acid, a kind of hard plastic, was chosen to construct the unit cells. The huge impedance contrast between air and solid ensures the validity of the assumption of sound hard boundary. The SCs were connected with super glue, with the joints further sealed with vacuum grease to minimize loss. The loudspeaker placed at one end of the waveguide emits a white noise and sound absorbing foam was mounted at the other end of the waveguide to eliminate the undesired reflections. A B&K type 2670

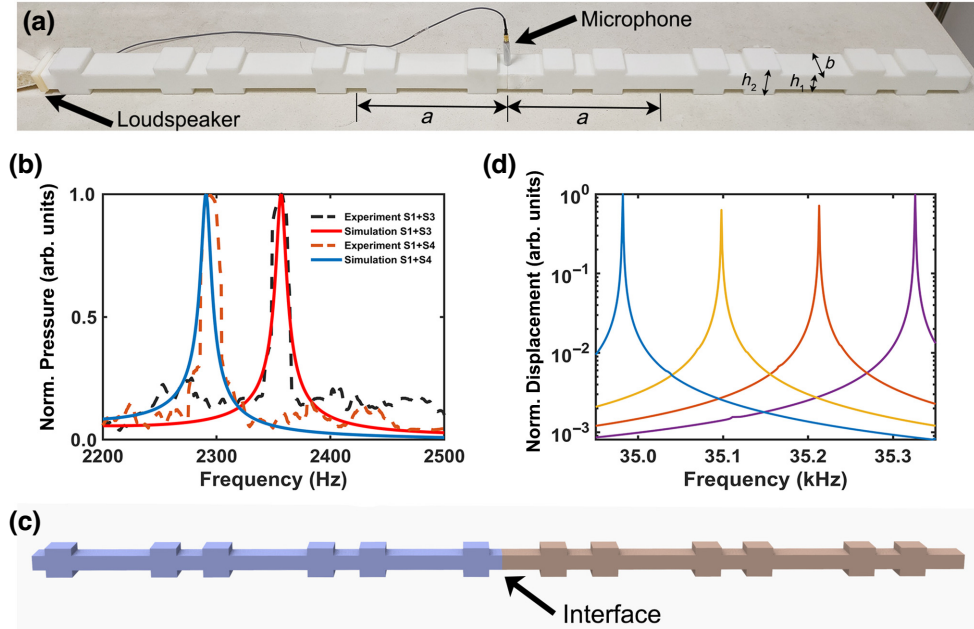


FIG. 5. (a) Photograph of the 3D-printed experimental setup composed of topologically different configurations. (b) Distribution of normalized acoustic pressure amplitude in our system obtained in both experimental measurements and numerical simulations for S1 + S3 and S1 + S4, respectively. The topological interface states exhibit a clear shift in topological band gap due to the breaking of double symmetry. (c) Schematic of the phononic aluminum beam composed of two topologically distinct PnCs (marked by different colors) and simulated distribution of normalized displacement at the topological interface states shown in (d).

microphone was placed at the interface of two SCs to measure the local acoustic field.

In Fig. 5(b), we show the distribution of normalized acoustic pressure amplitude in our system obtained in both experimental measurements and numerical simulations. There are interface states in the third band gaps of S1 + S3 (double symmetry) and S1 + S4 (symmetry breaking) at 2360 and 2291 Hz, respectively. Good agreement is observed between the numerical and experimental results, both showing a shift of the topological interface states within the band gap. The slight discrepancy in Fig. 5(b) results from unavoidable experimental errors related to imperfect sample fabrication and alignment, impedance mismatch at the waveguide end and nonuniform frequency response of the loudspeaker. Due to thermoviscous losses, our measured curves are not as sharp as those in simulation, and the field-enhancement performance can be further increased by improving the experimental setup to eliminate the undesired effect like the energy leak from waveguides in our system. The modulation of the topological interface states in a wide frequency range is expected to construct highly flexible acoustic broadband sensors and wave detectors. To test our approach in other wave-based systems, we engineer an elastic heterostructure out of PnCs that are composed of aluminum beams (density  $\rho_{\text{Al}} = 2700 \text{ kg/m}^3$ , Young's modulus  $E = 70 \times 10^9 \text{ Pa}$ ) as shown in Fig. 5(c). The geometric size of the PnC is the same as the acoustic setup and the velocity of the longitudinal wave  $c_L = \sqrt{E_{\text{Al}}/\rho}$ . Much like the acoustic counterpart, the ultrasonic heterostructure also produces multifrequency modulation of enhanced topological interface states as shown in Fig. 5(d). The colored curves indicate enhanced normalized displacement at different interface state frequencies and the sound pressure is normalized with respect to the maximal value of the simulated and measured sound pressure (normalization is performed for simulation and experiment, respectively).

## V. CONCLUSION

In this study, we present both theoretically and experimentally an acoustic heterostructure whose topological interface state can be tuned across the entire band gap. Through the adjustment of the coupling strength between the resonant cavities on both sides of the interface that depends only on a single structural parameter, we predict near-uniform intensity enhancements of the measured signal. We also test this mechanism using an ultrasonic phononic crystal, which also displays near-uniform vibrational intensity across its topological band gap. Our strategy of producing high and constant enhancement of local intensity at arbitrary frequency would be highly desired for many worthwhile applications such as acoustic noninvasive detection, which usually requires highly

sensitive detection of narrowband signals with varying central frequency.

## ACKNOWLEDGMENTS

This work was supported by the National Key R&D Program of China (Grants No. 2022YFA1404402 and No. 2017YFA0303700), the National Natural Science Foundation of China (Grants No. 12174190, No. 11634006, and No. 81127901), High-Performance Computing Center of Collaborative Innovation Center of Advanced Microstructures and A Project Funded by the Priority Academic Program Development of Jiangsu Higher Education Institutions.

- [1] Z. Gu, H. Gao, T. Liu, S. Liang, S. An, Y. Li, and J. Zhu, Topologically Protected Exceptional Point with Local Non-Hermitian Modulation in Acoustic Crystal, *Phys. Rev. Appl.* **15**, 014025 (2021).
- [2] G. Ma, M. Xiao, and C. T. Chan, Topological phases in acoustic and mechanical systems, *Nat. Rev. Phys.* **1**, 281 (2019).
- [3] M. Z. Hasan and C. L. Kane, Colloquium: Topological insulators, *Rev. Mod. Phys.* **82**, 3045 (2010).
- [4] M. Xiao, G. Ma, Z. Yang, P. Sheng, Z. Q. Zhang, and C. T. Chan, Geometric phase and band inversion in periodic acoustic systems, *Nat. Phys.* **11**, 240 (2015).
- [5] Q. Wang, M. Xiao, H. Liu, S. Zhu, and C. T. Chan, Measurement of the Zak phase of photonic bands through the interface states of a metasurface/photonic crystal, *Phys. Rev. B* **93**, 041415(R) (2016).
- [6] H. Xue, Y. Ge, H. X. Sun, Q. Wang, D. Jia, Y. J. Guan, S. Q. Yuan, Y. Chong, and B. Zhang, Observation of an acoustic octupole topological insulator, *Nat. Commun.* **11**, 2442 (2020).
- [7] A. B. Khanikaev, R. Fleury, S. H. Mousavi, and A. Alu, Topologically robust sound propagation in an angular-momentum-biased graphene-like resonator lattice, *Nat. Commun.* **6**, 8260 (2015).
- [8] J. Lu, C. Qiu, L. Ye, X. Fan, M. Ke, F. Zhang, and Z. Liu, Observation of topological valley transport of sound in sonic crystals, *Nat. Phys.* **13**, 369 (2016).
- [9] R. Süsstrunk and S. D. Huber, Observation of phononic helical edge states in a mechanical topological insulator, *Science* **349**, 47 (2015).
- [10] H. Xue, Y. Yang, F. Gao, Y. Chong, and B. Zhang, Acoustic higher-order topological insulator on a kagome lattice, *Nat. Mater.* **18**, 108 (2019).
- [11] C. L. Kane and T. C. Lubensky, Topological boundary modes in isostatic lattices, *Nat. Phys.* **10**, 39 (2013).
- [12] C. He, X. Ni, H. Ge, X. C. Sun, Y. B. Chen, M. H. Lu, X. P. Liu, and Y. F. Chen, Acoustic topological insulator and robust one-way sound transport, *Nat. Phys.* **12**, 1124 (2016).
- [13] W. Zhu, X. Fang, D. Li, Y. Sun, Y. Li, Y. Jing, and H. Chen, Simultaneous Observation of a Topological Edge State and

- Exceptional Point in an Open and Non-Hermitian Acoustic System, *Phys. Rev. Lett.* **121**, 124501 (2018).
- [14] Q. Guo, T. Jiang, R. Y. Zhang, L. Zhang, Z. Q. Zhang, B. Yang, S. Zhang, and C. T. Chan, Experimental observation of non-Abelian topological charges and edge states, *Nature* **594**, 195 (2021).
- [15] M. Xiao, Z. Q. Zhang, and C. T. Chan, Surface Impedance and Bulk Band Geometric Phases in One-Dimensional Systems, *Phys. Rev. X* **4**, 021017 (2014).
- [16] L. S. He, H. W. Guo, Y. B. Jin, X. Y. Zhuang, T. Rabczuk, and Y. Li, Machine-learning-driven on-demand design of phononic beams, *Sci. China Phys. Mech. Astron.* **65**, 214612 (2022).
- [17] L. Feng, R. El-Ganainy, and L. Ge, Non-Hermitian photonics based on parity-time symmetry, *Nat. Photonics* **11**, 752 (2017).
- [18] F. D. Haldane and S. Raghu, Possible Realization of Directional Optical Waveguides in Photonic Crystals with Broken Time-Reversal Symmetry, *Phys. Rev. Lett.* **100**, 013904 (2008).
- [19] G. Cáceres-Aravena, B. Real, D. Guzmán-Silva, A. Amo, L. E. F. Torres, and R. A. Vicencio, Experimental observation of edge states in SSH-stub photonic lattices, *Phys. Rev. Res.* **4**, 013185 (2022).
- [20] F. Gao, S. H. Xue, Z. Yang, K. Lai, Y. Yu, X. Lin, Y. Chong, G. Shvets, and B. Zhang, Topologically protected refraction of robust kink states in valley photonic crystals, *Nat. Phys.* **14**, 140 (2018).
- [21] M. Li, D. Zhirihin, M. Gorlach, X. Ni, D. Filonov, A. Slobozhanyuk, A. Alù, and A. B. Khanikaev, Higher-order topological states in photonic kagome crystals with long-range interactions, *Nat. Photonics* **14**, 89 (2020).
- [22] M. Atala, M. Aidelsburger, J. T. Barreiro, D. Abanin, T. Kitagawa, E. Demler, and I. Bloch, Direct measurement of the Zak phase in topological Bloch bands, *Nat. Phys.* **9**, 795 (2013).
- [23] J. Yin, M. Ruzzene, J. Wen, D. Yu, L. Cai, and L. Yue, Band transition and topological interface modes in 1D elastic phononic crystals, *Sci. Rep.* **8**, 6806 (2018).
- [24] L. Wang, W. Cai, M. Bie, X. Zhang, and J. Xu, Zak phase and topological plasmonic Tamm states in one-dimensional plasmonic crystals, *Opt. Express* **26**, 28963 (2018).
- [25] E. J. Meier, F. A. An, and B. Gadway, Observation of the topological soliton state in the Su–Schrieffer–Heeger model, *Nat. Commun.* **7**, 13986 (2016).
- [26] X. Li, Y. Meng, X. Wu, S. Yan, Y. Huang, S. Wang, and W. Wen, Su–Schrieffer–Heeger model inspired acoustic interface states and edge states, *Appl. Phys. Lett.* **113**, 203501 (2018).
- [27] W. Zhu, Y. Q. Ding, J. Ren, Y. Sun, Y. Li, H. Jiang, and H. Chen, Zak phase and band inversion in dimerized one dimensional locally resonant metamaterials, *Phys. Rev. B* **97**, 195307 (2018).
- [28] S. Puri, J. Ferdous, A. Shakeri, A. Basiri, M. Dubois, and H. Ramezani, Tunable Non-Hermitian Acoustic Filter, *Phys. Rev. Appl.* **16**, 014012 (2021).
- [29] M. Wang, W. Zhou, L. Bi, C. Qiu, M. Ke, and Z. Liu, Valley-locked waveguide transport in acoustic heterostructures, *Nat. Commun.* **11**, 3000 (2020).
- [30] X. Ni, M. Weiner, A. Alù, and A. B. Khanikaev, Observation of higher-order topological acoustic states protected by generalized chiral symmetry, *Nat. Mater.* **18**, 113 (2019).
- [31] Y. J. Ding, Y. G. Peng, Y. F. Zhu, X. D. Fan, J. Yang, B. Liang, X. F. Zhu, X. G. Wan, and J. C. Cheng, Experimental Demonstration of Acoustic Chern Insulators, *Phys. Rev. Lett.* **122**, 014302 (2019).
- [32] Z. Wang, D. Zhao, J. Luo, R. Wang, and H. Yang, Broadband modulation of subwavelength topological interface states in a one-dimensional acoustic system, *Appl. Phys. Lett.* **116**, 013102 (2020).
- [33] Z. Gu, H. Gao, P. C. Cao, T. Liu, X. F. Zhu, and J. Zhu, Controlling Sound in Non-Hermitian Acoustic Systems, *Phys. Rev. Appl.* **16**, 057001 (2021).
- [34] Q. Zhang, Y. Chen, K. Zhang, and G. Hu, Dirac degeneracy and elastic topological valley modes induced by local resonant states, *Phys. Rev. B* **101**, 014101 (2020).
- [35] H. Kazemi, M. Y. Nada, T. Mealy, A. F. Abdelshafy, and F. Capolino, Exceptional Points of Degeneracy Induced by Linear Time-Periodic Variation, *Phys. Rev. Appl.* **11**, 014007 (2019).
- [36] S. S. Tong, C. Y. Ren, and J. Tao, Compact topological waveguide for acoustic enhanced directional radiation, *Appl. Phys. Lett.* **120**, 063504 (2022).
- [37] D. Zhao, M. Xiao, C. W. Ling, C. T. Chan, and K. H. Fung, Topological interface modes in local resonant acoustic systems, *Phys. Rev. B* **98**, 014110 (2018).
- [38] W. Zhang, D. Zou, Q. Pei, W. He, J. Bao, H. Sun, and X. Zhang, Experimental Observation of Higher-Order Topological Anderson Insulators, *Phys. Rev. Lett.* **126**, 146802 (2021).
- [39] X. Jiang, C. Jiang, Z. Li, S. Wang, Y. Wang, S. Yang, S. G. Louie, and X. Zhang, Direct observation of Klein tunneling in phononic crystals, *Science* **370**, 1447 (2020).
- [40] X. J. Zhang, M. Xiao, Y. Cheng, M. H. Lu, and J. Christensen, Topological sound, *Commun. Phys.* **1**, 97 (2018).